Electrical dual-percolation in MWCNTs filled SBS/PVDF thermoplastic elastomer (TPE) composites and the effect of mechanical stretching

Christopher Ellingford[1], Henry Smith[1], Xue Yan[2], Christopher Bowen[3], Łukasz Figiel[1], Tony McNally[1], Chaoying Wan*[1]

[1]*International Institute for Nanocomposites Manufacturing (IINM), WMG, University of Warwick, CV4 7AL, UK*

[2]*Science and Technology on Advanced Functional Composites Laboratory, Aerospace Research Institute of Materials & Processing Technology, Beijing 100076, People's Republic of China*

[3]*Department of Mechanical Engineering, University of Bath, BA2 2ET, UK*

Corresponding author: C. Wan, Email: Chaoying.wan@warwick.ac.uk

Abstract

Dielectric thermoplastic elastomers (TPEs) offer a number of advantages over traditional dielectric elastomers or rubbers in terms of tailorable mechanical and electrical properties, higher mechanical strain, and ease of processing and shaping. Such a combination of properties has attracted increasing attention in flexible energy harvesting and storage applications. The combination of styrene-butadiene-styrene (SBS) and poly(vinylidene fluoride) (PVDF) has the potential to provide a combination of high elongation to break and increased relative permittivity, however the immiscibility between SBS and PVDF results in the polymer blends with poor stretchability and processing properties. In this work, a dual percolated structure was created in a thermoplastic elastomer of SBS/PVDF (50/50 wt%), by coupling EVA as a compatibiliser for SBS/PVDF with multi-walled carbon nanotubes (MWCNTs) as a conductive filler that created percolation electrical network. The elongation at break of SBS/PVDF was significantly enhanced by adding 20 wt% of EVA due to the reduced phase dimensions and enhanced interfacial adhesion. The addition of MWCNTs enabled the formation of a percolation network at 1 wt% in the SBS phase, followed by a second percolation at 3 wt% in both PVDF and SBS phases. The relative permittivity of the composite increased to 22.5 at 1 wt% MWCNT with a *tan δ* of 0.5, and further increased to 34.9 with 2 wt% of MWCNT concentration while the *tan δ* remained constant. *In-situ* electrical testing for the SBS/PVDF thermoplastic elastomer under strain showed that, at 1 wt% MWCNT, the non-percolated PVDF islands acted as variable capacitors whose capacitance increased with degree of

stretching. For the dual percolated structure formed at 3 wt% of MWCNT, the capacitance and conductivity of the composites were unaffected up to 30% strain. The high relative permittivity and strains of over 100% means that the SBS/PVDF thermoplastic elastomer is readily suitable for vibration control sensors, variable impedance devices, energy harvesters and artificial muscles and actuators.

Highlights

- Super compatibilisation and modification effects of EVA for SBS/PVDF thermoplastic elastomers investigated
- Dual percolation network that forms depends on the MWCNTs concentration and phase morphology of the polymer blends
- The dual percolated structure enhanced the relative permittivity and supressed the dielectric loss, and was not disrupted up to an elongation at break at 30% strain
- Rheological dual percolation agreed with electrical dual percolation thresholds

Key Words

thermoplastic elastomer; compatibility; dielectric properties; composite; double percolation threshold

Introduction

Dielectric elastomers are a class of electroactive polymers able to initiate a mechanical deformation in response to an electric field or convert structural deformation into an electrical output whilst operating under an applied field.[1] This electromechanical behaviour makes dielectric elastomers of great interest for energy harvesting, actuation, artificial muscles and as sensors.[2, 3] However, large voltages, and associated electric fields, are required to drive dielectric elastomers with potential differences of up to 10 kV.[4] This issue primarily stems from the low relative permittivity (ε_r) of dielectric elastomers (i.e. ε_r ~ 2-3). However, both relative permittivity and the drive voltage are key for developing actuating materials that can undergo large strains, as seen from equation 1:[5]

$$S = \frac{\varepsilon_0 \varepsilon_r}{Y}\left(\frac{V}{d}\right)^2 \qquad (1)$$

where S is the uniaxial strain component induced by the applied field, ε_0 is permittivity of free space, Y is the modulus of elasticity, V is the applied electric potential and d is the thickness of the sample.[5]

Ferroelectric poly(vinylidene fluoride) (PVDF) has a high relative permittivity of $\varepsilon_r \sim 12$, due to its highly polar chains, and a high breakdown strength, typically 590 MV m^{-1}.[6] The high breakdown strength allows the material to be subjected to a high electric field without breakdown. In addition, poled semicrystalline PVDF is piezoelectric due to the polarity and charge distribution of the VDF units[1], and in energy harvesting devices, piezoelectricity can be used as an initial charge input for the first cycle. As an example, a piezoelectric PVDF energy harvesting device was able to harvest 112.8 μW at 35 Hz, which represented an energy density of 8.61 mW cm^{-3}. The energy harvesting in this device was reported to be as high as ceramic based piezoelectric energy harvesting devices.[7]

However, the feasibility of use for PVDF for large-strain applications is limited by its mechanical properties, most notably a low elongation at break (10%) and high elastic modulus.[6, 8] Therefore, the blending of PVDF with a dielectric elastomer to form a PVDF thermoplastic elastomer (TPE) could elicit a material with appropriate electrical properties, such as high permittivity and high elongation at break. Unfortunately, PVDF is incompatible with many dielectric elastomers such as styrene-butadiene-styrene (SBS) and can lead to large phase dimensions and poor mixing.[9]

To increase the phase mixing between the two phases, PVDF can be dynamically vulcanised with acrylonitrile butadiene rubber to make a TPE with enhanced mechanical properties.[10] The crosslinks are formed during the melt mixing procedure to physically attach the two phases[11] and the resulting polymers are termed thermoplastic vulcanises (TPVs). An alternative to TPVs is to introduce a third polymer which is able to interact with both polymer phases and reside at the interface between the two.[12] Poly(methyl methacrylate) (PMMA) has been used to effectively compatibilise PVDF and polycarbonate blends, however, it was necessary to use 20-40 wt% of PMMA. A copolymer of PMMA, methyl methacrylate-co-glycidyl methacrylate (MMA-co-GMA) has also been used to compatibilise PVDF and polyamide 6 (PA6). The epoxy groups of glycidyl methacrylate interacted with the carboxy and amino groups of PA6 and characterisation showed that the crystallinity of both PVDF and PA6 was reduced by compatibilisation. However, the elongation at break of PVDF/PA6 increased from 20% to 250% after the introduction of MMA-

co-GMA.[13] Similarly, a poly(amide) 11 and PVDF blend was compatibilised through the addition of a vinyl acetate-maleic anhydride copolymer.[14] A final approach to increase phase mixing is to chemically functionalise PVDF. One such example is to compatibilise thermoplastic polyurethane with maleic anhydride (MA) grafted PVDF [15]; for example the fabrication of a wind energy harvesting device utilising both PVDF and an elastomer to produce a flexible piezoelectric sheet resulted in a maximum energy density of 200 mW m^{-2}.[16]

The addition of a conductive filler to a thermoplastic elastomer in an effort to further tailor the electrical properties can alter the phase morphology of blends, reduce the flexibility and elongation of a composite. It can also affect the electrical properties by increasing the conductivity and relative permittivity of the composite. Therefore, it is desirable to incorporate a minimal amount of filler for the highest electrical properties. The incorporation of partially reduced graphene-oxide into PVDF increased the relative permittivity to a maximum of $\varepsilon_r \sim 225$.[17] However, the introduction of conductive carbon fillers increases the dielectric loss of the composite significantly due to an increase in the leakage current.[18] This is more pronounced after the formation of a percolation network, and the breakdown strength is reduced due to inhomogeneous electric fields present within the polymer matrix.[19] In polymer blends, a double percolation event can be observed in which a material undergoes two network formations to result in a two-step increase in electrical conduction and relative permittivity. This arises due to the selective localisation of the filler in one phase of the blend over the other, resulting in percolation in one phase before the other,[20] as a result of inhomogeneous filler distribution. When a double percolation event can take place, the first percolation event is typically observed at a lower than normal filler concentration.[21]

In this paper, we investigate the relationship of structure and properties of thermoplastic elastomer (TPE) composites of SBS/PVDF with multi-walled carbon nanotubes (MWCNTs), in which ethylene vinyl acetate (EVA) was used as a compatibiliser. The effects of the compatibiliser and MWCNT on the mechanical, electrical and rheological properties of the TPE composites are investigated. The enhancement of the dielectric properties of the TPE composites and the change in dielectric properties during mechanical stretching are discussed, since the material is likely to be subjected to high strain when used as an actuator or harvester. The materials are also subjected to in-depth characterisation of the crystalline structures and phase morphology of PVDF. This work shows the first successful formation of a SBS/PVDF TPE with EVA as a compatibiliser to

result in good mechanical properties and high relative permittivity, whilst maintaining a low dielectric loss followed by its subsequent compositing.

Experimental

Materials

Styrene-butadiene-styrene (SBS, Vector 8508A) was purchased from Dexco. Poly(vinylidene fluoride) (PVDF, Kynar 740) was purchased from Arkema. Ethylene vinyl acetate (EVA, ELVAX 3190) was purchased from DuPont. Non-functionalised thin multi-walled carbon nanotubes (MWCNTs) produced by catalytic carbon vapour deposition (grade NC7000, purity > 90%) were purchased from Nanocyl S.A., Belgium. The MWCNTs had an average diameter of 9.5 nm, average length of 1.5 μm and a density of 1.85 g cm^{-3}.[22] Carbon black grease was purchased from MG Chemicals, UK, to act as a compliant electrode for electrical studies.

Preparation

SBS/PVDF (50/50 wt%) and EVA compatibilised SBS/PVDF (50/50) were prepared by melt-blending using a HAAKE Rheomix OS Lab Mixer at 190 °C, 60 rpm for 10 mins. The EVA content was 20 wt% of SBS/PVDF (50/50), denoted as SBS/PVDF/EVA (50/50/20) in this work. 0.3 ~ 3 wt% of MWCNTs were added to the composites, based on the total weight of the SBS/PVDF/EVA blends and are denoted as 50/50/20/X, where X is the MWCNT wt%. The samples were then compression moulded using a Rondol manual hot press at 190 °C and 10 kN.

Characterisation

Scanning electron microscopy (SEM) imaging was performed using a Carl Zeiss Sigma Field SEM on cryofractured samples which were sputter coated using an Au/Pd target. Dynamic Mechanical Thermal Analysis (DMTA) was performed on samples 5.0 mm × 10.0 mm × 1 mm in single cantilever mode with a 50 μm amplitude and a frequency of 1 Hz using a Triton Tritec 2000 DMA. For EVA the temperature range of -120 °C to 60 °C was used and for all other samples the temperature range was -120 °C to 135 °C. Differential Scanning Calorimetry measurements were carried out using a Mettler Toledo DSC1 Star^{e} between -40 °C and 225 °C at a heating and cooling rate of 10 °C min^{-1} for two cycles. Fourier transform infrared spectroscopy (FT-IR) was recorded using a Bruker Tensor 27 at a resolution of 4 cm^{-1} with 32 scans for the background and the samples. Contact Angle measurements were recorded using an Attension Theta Lite using H_2O and CH_2I_2 as the wetting solvents. Liquid drops of 2.5 μl were recorded on samples for a 3-second

period and the contact angle averaged over the period. Oscillatory Rheometry was tested using a HAAKE MarsIII Rheometer at 190 °C with a frequency range of 0.1 to 100 Hz. Impedance spectroscopy measurements were carried out using a Princeton Applied Research Parstat MC with a PMC-2000 card and a two-point probe between 10^0~10^6 Hz on thin films of thickness between 100~200 μm and an electrode area of 5 cm × 5 cm. Samples were examined in terms of their Polarisation-Electric Field (P-E) response using a Radiant RT66B-HVi Ferroelectric Test system at room temperature with a maximum applied potential of 4kV and a test duration of approximately 10ms; the applied voltage (and associated electric field) was gradually increased to the maximum value. The sample test areas were approximately 1.3-1.5cm^2, and their thickness were 1.09-1.21mm. The upper and lower surfaces of the material were covered by silver electrodes (Product No.186-3600) to form electrical contacts.

Mechanical testing was performed using a Shimadzu Autograph AGS-X tester with samples conforming to ASTM-D638-14 type V. The extension rate was 50 mm min^{-1} (nominal strain rate = 0.1095 s^{-1}) with a 10 kN load cell and tests were carried out at room temperature. Stress relaxation was investigated by stretching the tensile specimens to 100% nominal strain at 50 mm min^{-1} and holding the samples at constant strain until the stress reached equilibrium. Cyclic stress softening was performed by deforming specimens to 100% strain and back to 0% under a controlled elongation rate of 50 mm min^{-1} for 5 cycles. To examine the frequency dependent electrical properties as a function of strain, the dogbone samples were fitted into a Hounsfield test machine with small wires attached to the gauge length of sample via a small bead of conductive epoxy. The electrode along the gauge length of the sample was then formed via a conductive carbon grease and connected to a Solatron 1260 and 1296 Dielectric Interface.

Results and Discussion

Compatibilisation of SBS/PVDF TPE

The elongation at break for PVDF is typically lower than 15 % due to its semi-crystalline nature. This limits its use in applications that require a polymer to have good electrical properties, such as high permittivity, and stretchability. Blending PVDF with SBS elastomer to produce a SBS/PVDF (50/50) TPE further reduced the elongation at break to 11%, due to the poor compatibility between the two polymers, see Figure 1. The selection of a compatibiliser is a key in modification of the properties of SBS/PVDF TPEs. In this work EVA was evaluated for compatibilising SBS/PVDF

blends, as such the addition of 20 wt% of EVA to SBS/PVDF (50/50) significantly increased the elongation at break to 205% and a tensile strength of 2.95 MPa.

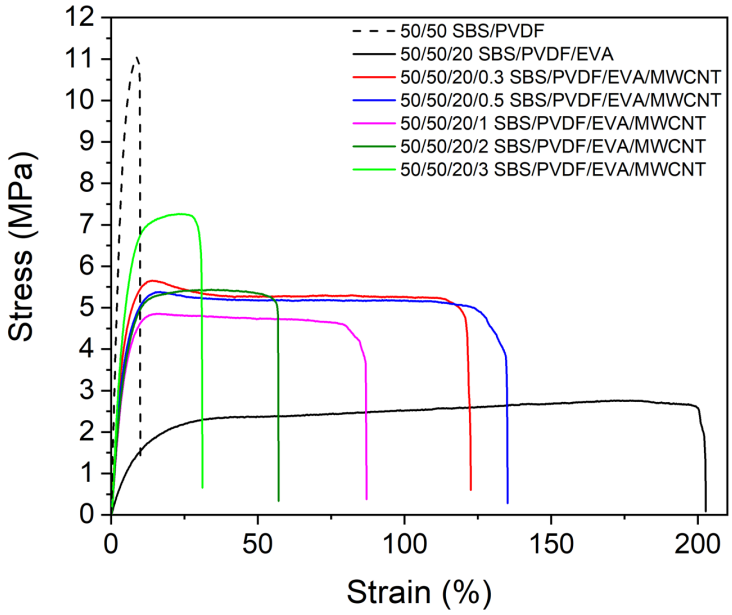

Figure 1 Characteristic stress-strain curves of SBS/PVDF/EVA and MWCNT containing composites.

DMTA was performed to evaluate the compatibilisation effect that EVA introduces to SBS/PVDF (50/50) blend, the storage modulus (E') and loss modulus (E'') in Figure 2a and 2b respectively are used to determine $tan\ \delta = E''/E'$ in Figure 2c which indicates the glass transition temperature (T_g) of the respective polymers in the blend. In SBS/PVDF, the peaks at -83.8 °C, -37.6 °C, 92.4 °C and 118.6 °C are attributed to the T_g of the butadiene block of SBS, PVDF, the styrene block and α-relaxation of PVDF, respectively.[23] The addition of 20 wt% EVA to SBS/PVDF noticeably affects the T_g's of the blend. Firstly, there is a minor increase in the T_g of the butadiene block from -83.8 °C to -80.4 °C, indicating a van der waals interaction between the butadiene block with the ethylene block of EVA. The T_g of PVDF at -37.6 °C was replaced by a broad hump with a peak value at -6.8 °C as the carbonyl groups on acetyl hydrogen bond with the fluoride groups of PVDF.[24] Since neat EVA should display a T_g at -17.4 °C, the shift in the T_g*'s* of the butadiene block and PVDF demonstrates the interaction of EVA with both SBS and PVDF, as seen in Figure 2D.

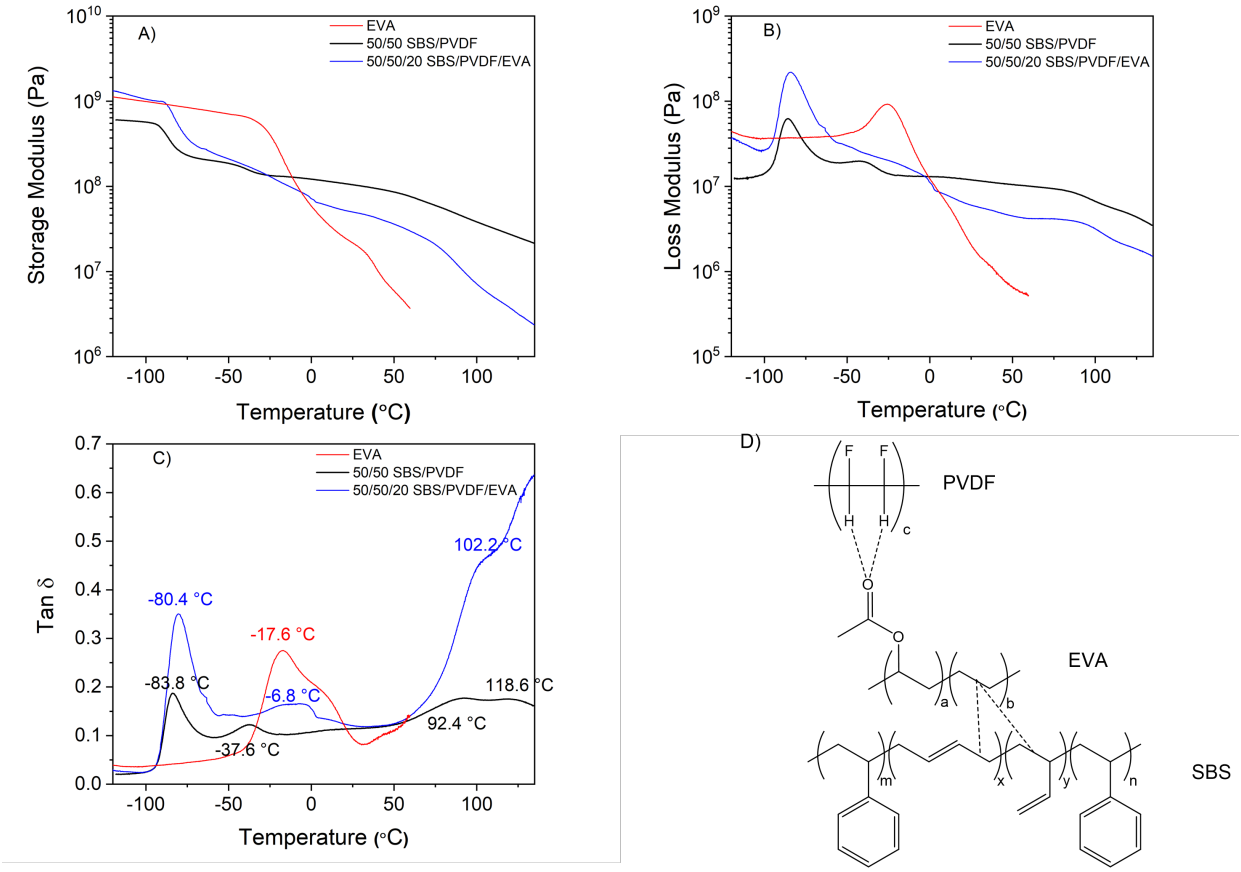

Figure 2: A) storage modulus of neat EVA, SBS/PVDF (50/50) and the compatibilised blend SBS/PVDF/EVA (50/50/20), B) the loss modulus of neat EVA and both blends, C) the *tan δ* of neat EVA and both blends showing the change in T_g upon addition of 20 wt% of EVA through its compatibilising effect and D) a diagram of the structures of SBS, EVA and PVDF and the interactions between SBS and PVDF with EVA

The compatibilisation effect of EVA is also reflected by the phase morphology change of the blends. As shown in Figure 3A, the dimensions of both SBS and PVDF phases were at scale of hundreds of micrometres and show clear phase separation. The addition of 20 wt% of EVA significantly reduced the phase dimensions of both SBS and PVDF and resulted in PVDF as long 'worm-like' and ovoid shapes in the SBS matrix (Figure 3B). SBS and EVA demonstrate good phase mixing due to the ethylene units interacting with the butadiene block. In addition, the EVA carbonyls interact through hydrogen bonding with PVDF,[24] thus ensuring EVA resides at the interface between PVDF and SBS (Figure 2D). This explains the stress-strain behaviour of the SBS/PVDF TPEs in Figure 1.

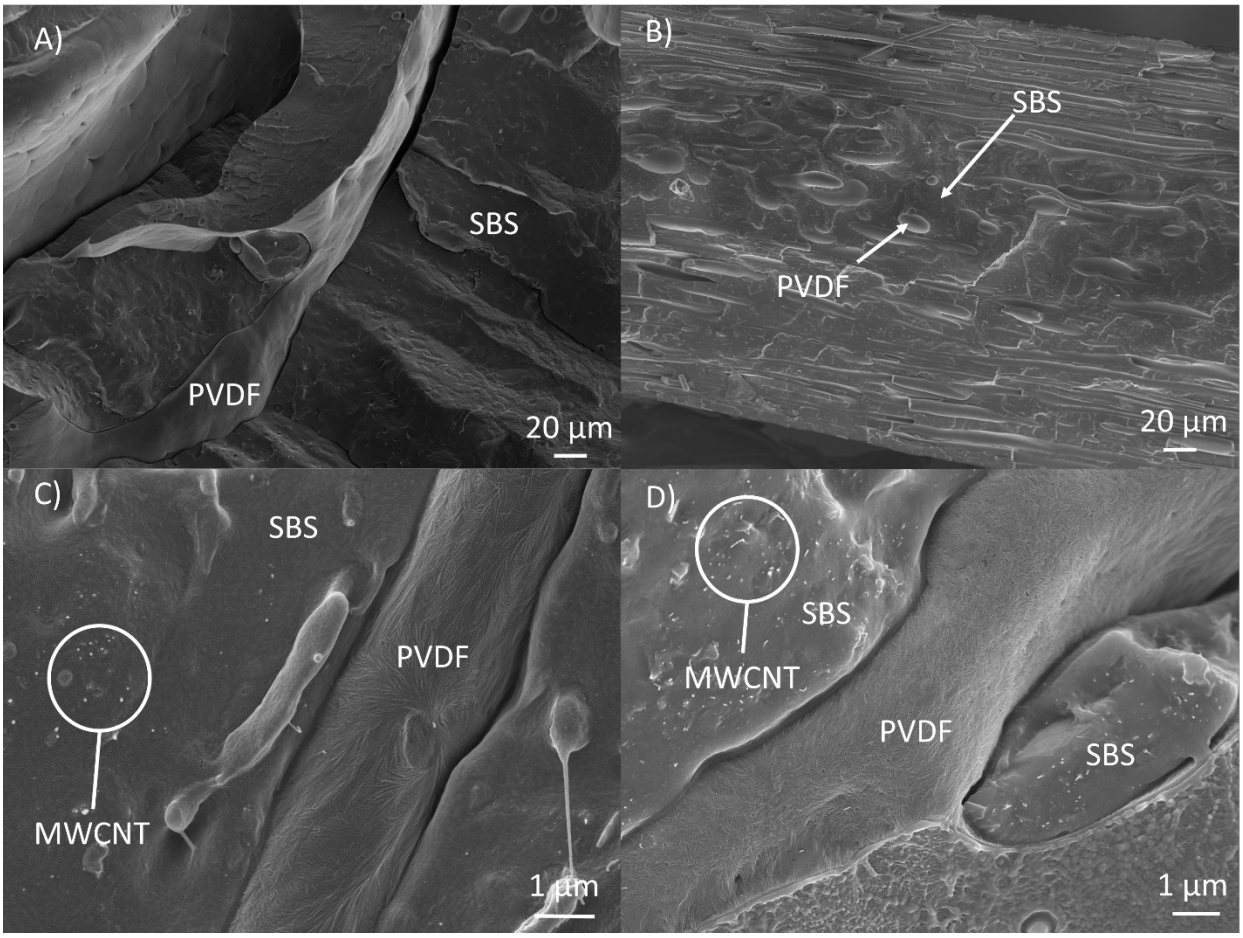

Figure 3: Phase morphology of (a) SBS/PVDF (50/50) showing phase separation, (b) SBS/PVDF/EVA (50/50/20), (c) SBS/PVDF/EVA/MWCNT (50/50/20/1) with MWCNTs selectively localised in the SBS phase and (d) SBS/PVDF/EVA/MWCNT (50/50/20/3) showing a growing phase separation between the SBS and PVDF phase.

Selective localisation of MWCNT in SBS/PVDF TPEs

The mechanical and electrical properties of SBS/PVDF TPEs will be affected by the dispersion of MWCNTs, in particular, the selection localisation of MWCNTs in either phase of SBS/PVDF/EVA. Contact angle measurements were carried out to provide theoretical evidence for the locality of the MWCNTs in the SBS/PVDF/EVA TPEs. The MWCNT exhibit a different affinity to the polymer phases, primarily through electrostatic interactions, π-π stacking or van der waals forces. To determine this, the wetting coefficient, ω_a, is calculated from the interfacial surface tensions between the MWCNTs and SBS, EVA and PVDF and from the interfacial surface tensions between the polymers, as shown in equation 2:[25]

$$\omega_a = \frac{\gamma_{MWCNTs-polymer1} - \gamma_{MWCNTs-polymer2}}{\gamma_{polymer1,2}} \quad (2)$$

where $\gamma_{MWCNTs\text{-}polymer1}$ is the interfacial tension between MWCNTs and Polymer 1, $\gamma_{MWCNTs\text{-}polymer2}$ is the interfacial tension between MWCNTs and Polymer 2 and $\gamma_{polymer1,2}$ is the interfacial tension between Polymer 1 and 2. As such,

(i) when $\omega_a < 1$, the MWCNTs prefer to reside in Polymer 1,

(ii) if ω_a is between 0 and 1 then the MWCNTs are at the interface between both polymers and,

(iii) if ω_a is > 1, the MWCNTs prefer to reside in Polymer 2.

The interfacial tension between the two components is calculated using the geometric mean in equation 3:[26]

$$\gamma_{1,2} = \gamma_1 + \gamma_2 - 2\left(\sqrt{\gamma_1^d \gamma_2^d} + \sqrt{\gamma_1^p \gamma_2^p}\right) \quad (3)$$

where γ_i is the total surface energy of component *i* and γ_i^d and γ_i^p are the dispersive and polar parts of the surface energy of component *i* respectively. To calculate the surface energy, the geometric mean method was used, as shown in equation 4 and 5:[27]

$$\gamma_{LV} = (1 + cos\theta) = 2\left(\sqrt{\gamma_{SV}^d \gamma_{LV}^d} + \sqrt{\gamma_{SV}^p \gamma_{LV}^p}\right) \quad (4)$$

$$\gamma_{SV} = \gamma_{SV}^d + \gamma_{SV}^p \quad (5)$$

where θ is the observed contact angle, γ_{SV} and γ_{LV} are interfacial surface-vapour and liquid-vapour respectively, and the respective superscripts *d* and *p* are for the disperse and polar components of surface tension. For the contact angle measurements, distilled H_2O and CH_2I_2 were chosen. The surface energy data of the solvents are shown in Table 1.[28]

Table 1 Surface energy data of H_2O and CH_2I_2;[28] superscripts *d* and *p* are for the disperse and polar components of surface tension.

Solvent	γ_{LV} **[N m^{-1}]**	γ_{LV}^d **[N m^{-1}]**	γ_{LV}^p **[N m^{-1}]**
H_2O	72.8	21.8	51.0

CH_2I_2	50.8	48.5	2.3

The observed contact angles for SBS, PVDF and EVA are shown in Table 2. The wetting coefficient, ω_a, was calculated using equations 2 – 5 and the theoretical interfacial tension for MWCNTs[29]. Table 3 shows the results obtained to determine which polymers the MWCNTs prefer to reside in. From the contact angle measurements, the MWCNTs preferentially reside in both SBS and the SBS/EVA interface.

Table 2 Measured contact angle of SBS, PVDF and EVA in both H_2O and CH_2I_2

Material	**θ for H_2O [°]**	**θ for CH_2I_2 [°]**
SBS	98.8	72.4
PVDF	102.2	67.2
EVA	94.2	63.9

Table 3 Calculated wetting coefficient, ω_a, of the polymer systems and the preferred residence of MWCNTs, calculated from equations 2 – 5

Polymer 1	**Polymer 2**	**ω_a**	**Preferred Polymer**
PVDF	SBS	1.3190	SBS
EVA	SBS	0.6658	SBS/EVA
PVDF	EVA	5.82	EVA

SEM imaging in Figure 3C and D shows experimentally the locality of the MWCNTs upon compositing the thermoplastic elastomer. MWCNTs reside in the SBS phase and as the concentration of MWCNTs is increased, a gap is formed between the SBS matrix and the EVA/PVDF phase. The phase dimensions of the EVA/PVDF phase also increase in size. This suggests that the presence of the MWCNTS at the SBS/EVA interface reduced the compatibility between SBS and EVA. The decrease in compatibility is rationalised by considering the interactions present between SBS and MWCNTs. MWCNTs interact through π-π stacking with the styrene portion. However, during melt mixing the butadiene section undergoes oxidative

degradation to form free radicals. These free radicals can react with open MWCNT ends and defects.[30, 31] As the number of MWCNTs present increases, the degree of MWCNT bonding with the butadiene block increases, reducing the availability of butadiene to interact with the ethylene units of EVA.

The effect of MWCNTs on the compatibility of the TPEs is also demonstrated in the stress-strain curves in Figure 1. The addition of 0.3 wt%, 0.5 wt% and 1 wt% MWCNTs further increased the tensile strength of SBS/PVDF/EVA from 2.95 MPa to approximately 4.5 MPa. However, this reduced the elongation at break of the PVDF TPE from 205% to 110%, 127% and 111% respectively for the three samples. The MWCNTs reduced the elasticity of the SBS component due to their π-π interactions with the styrene block and the reinforcement of the butadiene block *via* the alkene groups,[30, 31] which inhibits the compatibilisation of SBS with EVA.

Further increasing the MWCNT concentration to 2 wt% significantly decreased the elongation at break to 61.7%, which is a result of the increased incompatibility between SBS and PVDF. Finally, with a 3 wt% of MWCNTs in the composite, the tensile strength increased significantly to 7.48 MPa and a further reduction in the elongation at break to 30.6%.

Stress relaxation testing was performed on the TPE and composites with an elongation at break of greater than 100%. This investigated how the MWNCTs affected the stress relaxation behaviour of the network of entangled polymer chains due to slipping over time. The percentage (%) of maximum stress of the composites, at time = 0 mins, decreased in a similar way for all materials tested, and reached between 45 and 48% of the maximum stress after 60 minutes, see Figure 4A. This showed that the MWCNTs had a minimal impact on the entanglement of the polymer chains in the composites within the investigated time range.

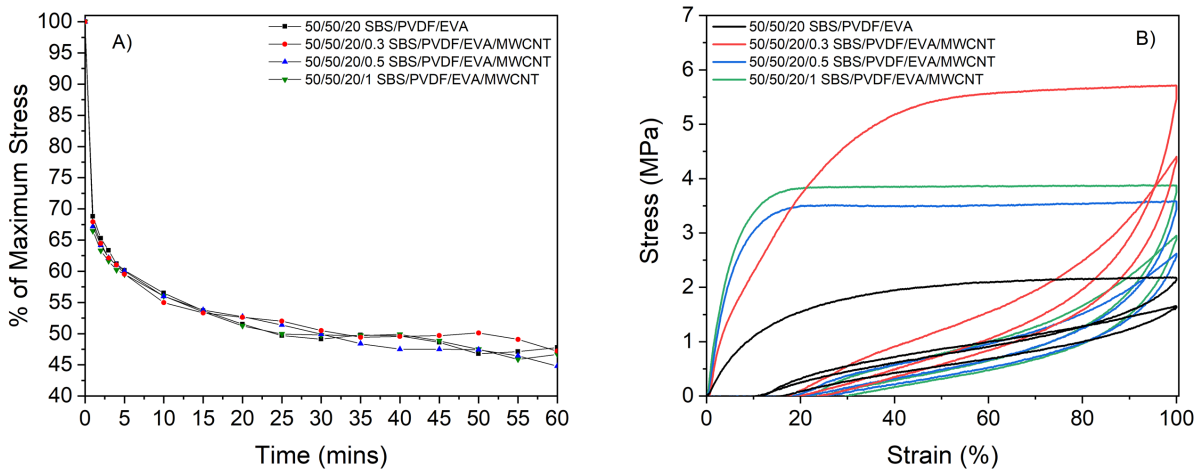

Figure 4: A) The decrease in stress as a comparative percentage to maximum stress against time. B) Cyclic stress softening curves of the first and fifth cycle for SBS/PVDF/EVA (50/50/20) and MWCNT containing composite blends.

The effect of MWCNTs on the hysteresis energy loss of the TPEs was investigated by cyclic tensile testing. All materials exhibit a pronounced hysteresis and cyclic stress softening, as can be seen in Figure 4B. For EVA compatibilised SBS/PVDF (50/50), the hysteresis energy loss is 55.4% after 5 cycles, showing the highly viscoelastic nature of this blend. The large loss is attributed to the energy dissipation within the TPE. As 0.3 wt% MWCNT are introduced into the composite, the hysteresis energy loss increases substantially to 70.1%, showing that the viscous portion of the composite has increased. Subsequently, as the MWCNT concentration increases further to 1 wt% the hysteresis energy loss continues to increase, albeit at a slower rate, and reached 75%. The increase in the viscous loss is attributed to the growing incompatibility between the polymer phases as MWCNT concentration increases, causing more damage in the polymer matrix on the first elongation.[32, 33]

The presence of the compatibiliser EVA and the selective localisation of MWCNTs in the blends affected the crystalline structures of PVDF. DSC was used to determine the change in percentage crystallinity, X_c(%), of PVDF and EVA upon increasing concentration of the MWCNTs, where the heat of fusion for 100% crystalline PVDF and EVA was taken to be 104.7 J g^{-1} and 277.1 J g^{-1} respectively.[34, 35]

Table 4 shows the X_c(%) changes upon formation of the SBS/PVDF/EVA TPE, compared to neat PVDF and EVA. This resulted in a large decrease in the X_c(%) compared to the neat polymers. The X_c(%) for PVDF decreased by 12.3% whereas X_c(%) for EVA decreased by 61.3%. This was attributed to the addition of EVA acting as a compatibiliser for SBS and PVDF, resulting in high concentrations of amorphous regions due to better phase mixing.

Table 4: DSC crystallinity data indicating how the components of SBS/PVDF/EVA (50/50/20) are affected by mixing and by compositing

Material	**X_c(%) PVDF**	**X_c(%) EVA**
PVDF	48.7	-
EVA	-	22.0
SBS/PVDF/EVA (50/50/20)	42.7	8.51
SBS/PVDF/EVA/MWCNTs (50/50/20/0.3)	45.1	8.70
SBS/PVDF/EVA/MWCNTs (50/50/20/0.5)	45.2	9.42
SBS/PVDF/EVA/MWCNTs (50/50/20/1)	45.0	11.0
SBS/PVDF/EVA/MWCNTs (50/50/20/2)	46.3	11.4
SBS/PVDF/EVA/MWCNTs (50/50/20/3)	47.4	11.8

The effect of compatibilisation on the degree of crystallinity (X_c %) of α-phase and β-phase in PVDF was studied by FTIR. Thus, the intensity of the two α-phase peaks at 763 cm^{-1} and 615 cm^{-1} were compared to the two β-phase peaks at 840 cm^{-1} and 1275 cm^{-1} respectively, seen in Figure S1. Table S1 details how the ratios between the peaks changes between neat PVDF and SBS/PVDF/EVA and demonstrates how the origins of crystallinity changes in PVDF. In neat PVDF, the β-phase has a greater intensity than the α-phase. However, by blending with SBS and EVA, the ferroelectric β-phase decreases whilst the non-polar α-phase increases to become more dominant. Some of the β-phase is converted to α-phase crystallinity whilst some regions become amorphous as observed by the decrease in X_c(%) from DSC.

DSC demonstrated that increasing the concentration of MWCNTs increased X_c(%) for both PVDF and EVA, as seen in Table 4. This is because MWCNTs are able to act as heterogeneous nucleating sites for crystallisation.[36] The addition of 0.3 wt% of MWCNTs resulted in an increase in X_c(%) for PVDF from 42.7% to 45.1% with a minimal change in EVA. Further increases in the MWCNT

concentration showed an increase in X_c(%) for EVA to 11.0% whilst the X_c(%) for PVDF remained constant. This fits well with the contact angle results, as the MWCNTs inhibit the interaction between SBS and EVA, reducing the compatibility between the two polymers and thus increased the X_c(%) of EVA. Further increases in MWCNT concentration show a smaller increase in X_c(%) for EVA and a much larger increases for PVDF as the MWCNTs begin to also reside in this polymer phase. The large change in X_c(%) between 1, 2 and 3 wt% MWCNT is observed in the mechanical properties through the significant reduction of the elongation at break, Figure 1.

Figure 5 shows how the α/β phase intensity ratio changes upon addition of MWCNTs and Table S1 shows FTIR peak intensity data in transmission mode. A higher concentration of α or β phase resulted in a stronger peak with a lower transmission value in the recorded spectra. Therefore, a higher concentration of α-phase crystallinity resulted in a decrease in the α/β phase intensity ratio and a higher concentration of β-phase increased the α/β intensity ratio.

Upon addition of 0.3 wt% of MWCNTs, the α/β phase intensity ratio increases demonstrating a small increase in the β-phase of PVDF. However, between the additions of 0.3 and 2 wt% of MWCNTs, the α/β ratio decreases between the two peak sets. This shows that the α-phase crystallinity in PVDF is growing slowly with respect to the β-phase. However, the addition of 3 wt% MWCNTs demonstrates a large decrease in the α/β intensity ratio. This is due to an increase in the α-phase compared to the β-phase and demonstrates that MWCNTs also reside in PVDF between 2 wt% and 3 wt% concentration.

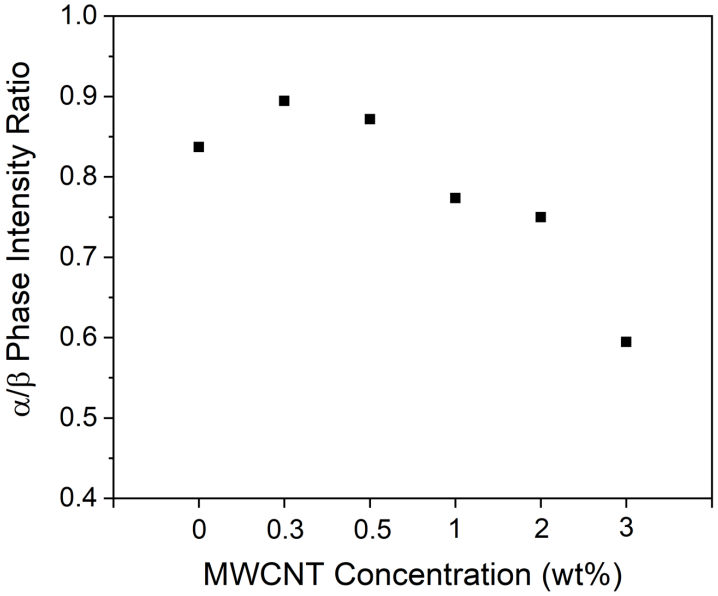

Figure 5: The change in the α/β phase intensity ratio with MWCNT concentration. A higher ratio value indicates more β-phase is present in PVDF.

Rheological dual-percolation characterisation

Oscillatory rheology was used to investigate the microstructure of the composites, see Figure 6. In these elastomeric composites, a large increase in the storage and loss modulus is observed between SBS/PVDF/EVA/MWCNT (50/50/20/0.5) and (50/50/20/1). This indicates that the increase of MWCNT addition starts to initiate a percolating network, and restricts polymer chain movement. Since the MWCNTs are mainly residing in the SBS phase, it demonstrates that a percolation threshold of MWCNTs was achieved between 0.5 and 1 wt%. The effect of the percolation threshold is most noticeable at low frequencies since at high frequencies the samples will tend to plateau.[22]

While the rheology demonstrates that the composites exhibit a second percolation event between SBS/PVDF/EVA/MWCNT (50/50/20/2) and (50/50/20/3), as there is a large increase in the storage and loss modulus for these samples. This may be explained by the migration of MWCNTs from SBS to PVDF phase at the higher concentration, and the formation of a second percolating network in the PVDF phase. The morphology of the composites with a range of MWCNTs concentrations are shown in Figure S2

Plotting the complex viscosity ($|\eta^*|$) vs frequency provides further evidence for reaching rheological percolation. The complex viscosity shows that the viscosity increases significantly in the samples at the two percolation events between 0.5 ~ 1 wt% and 2 ~ 3 wt% MWCNTs, as seen in Figure 6B. Therefore, a rheological double percolation structure was demonstrated.

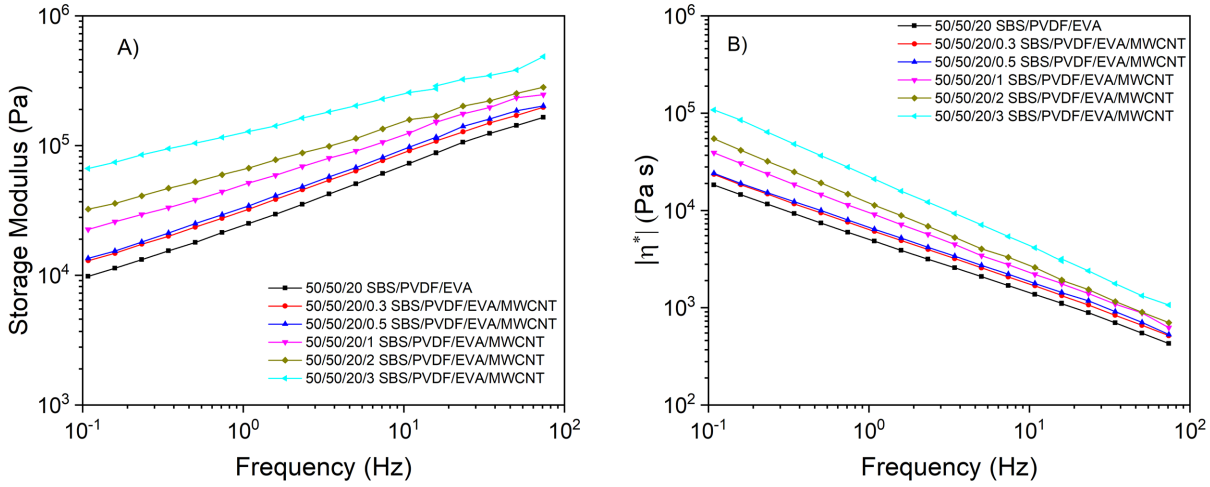

Figure 6: Rheology characterisation to show A) storage modulus against frequency and B) $|\eta^*|$ against frequency of SBS/PVDF/EVA (50/50/20) and MWCNT containing composites

Electrical dual-percolation characterisation

As shown in Figure 7, SBS/PVDF/EVA (50/50/20) had a low relative permittivity of ε_r ~ 3.8 at 10^3 Hz, which is only fractionally higher than neat SBS and EVA despite containing a significant portion of PVDF. This low ε_r fits well with DSC and FTIR results that the crystallinity decreases upon addition of EVA and that the α-phase becomes dominant at the expense of the β-phase, resulting in a low relative permittivity. For TPE composites, the relative permittivity increased to ε_r ~ 5.6 with an addition of 0.3 wt% of MWCNT. Both samples maintained a low electrical *tan δ*. A larger increase in relative permittivity to ε_r ~ 13.4 for 0.5 wt% MWCNT was observed, whilst the *tan δ* remained low at 0.1 at 10^3 Hz. This indicates that addition of 0.5 wt% of MWCNT nears the percolation threshold for the composite due to the characteristic rapid increase in relative permittivity, but low increase in *tan δ*. Once 1 wt% of MWCNT was added, the *tan δ* increased significantly to 0.5 at 10^3 Hz, with an increase in relative permittivity to ε_r ~ 22.5. The large

increase in the *tan δ* indicates that the first percolation threshold has been reached in the SBS phase. As such, the SBS/PVDF TPE composite exhibits a loss above a desirable level for low loss dielectric applications. Increasing the MWCNT concentration to 2 wt% further increased the relative permittivity to $\varepsilon_r \sim 34.9$, whilst the *tan δ* remained consistent at 0.47. As the *tan δ* remained constant, it demonstrated that the leakage current was suppressed by the insulating PVDF phase. This is evidenced by the increasing frequency dependency of the composites as the insulating PVDF phase firstly caused a build-up of charge at the interface of the polymer phases, increasing the Maxwell-Wagner-Sillars polarisation.[37] Secondly, the increase in MWCNTs introduced more voids and defects for space charge accumulation.

The suppression of *tan δ* after the first percolation event, accompanied by a high relative permittivity of up to $\varepsilon_r \sim 34.9$ and a strain at break of over 100%, means that the PVDF thermoplastic elastomer composite provides a combination of mechanical and electrical properties that make it readily suitable for vibration control sensors, variable impedance devices, energy harvesters and artificial muscles and actuators.[1] After the inclusion of 3 wt% of MWCNT, a second percolation event is observed for the PVDF phase. This caused the relative permittivity to increase to $\varepsilon_r \sim 395.0$ at 10^3 Hz with a very large *tan δ* of 123.8. This second percolation threshold is because of the localisation of a MWCNT network in the PVDF/EVA phase. The observation of the dual percolation events by both rheological (Figure 6) and electrical (Figure 7) characterisation indicates that the percolation of MWCNT influences both the electrical response and rheology of the composites.

The existence of a double percolation threshold in the elastomeric composites is further supported by the changes in the AC conductivity and phase angle between all of the samples. The addition of 0.3 wt% MWCNT showed a less than one order of magnitude increase in AC conductivity compared to 0 wt% of MWCNTs, from 1.8×10^{-9} S m^{-1} to 9.4×10^{-9} S m^{-1}. In addition, the phase angle showed that both samples remained fully insulating. Increasing the MWCNT concentration to 0.5 wt% increased the AC conductivity by another order of magnitude to 7.6×10^{-8} S m^{-1} and the sample showed a deviation from fully insulating in its phase angle at low frequencies as the composites began to develop a frequency dependency (< 100 Hz). The addition of 1 and 2 wt% of MWCNT yields similar AC conductivities at 6.3×10^{-7} S m^{-1} and 9.2×10^{-7} S m^{-1} respectively as the first percolation network had been formed in the SBS phase. The phase angle for both is almost identical across the frequency range and shows an insulating nature (90°) at high frequency which

tends to fully conducting at low frequency (0°). Finally, for inclusion of 3 wt% of MWCNT the second percolation event in the PVDF/EVA phase increased the conductivity by four orders of magnitude to 2.7 × 10^{-3} S m^{-1} at 10^3 Hz. The phase angle shows that the sample was conductive across the entire frequency range.

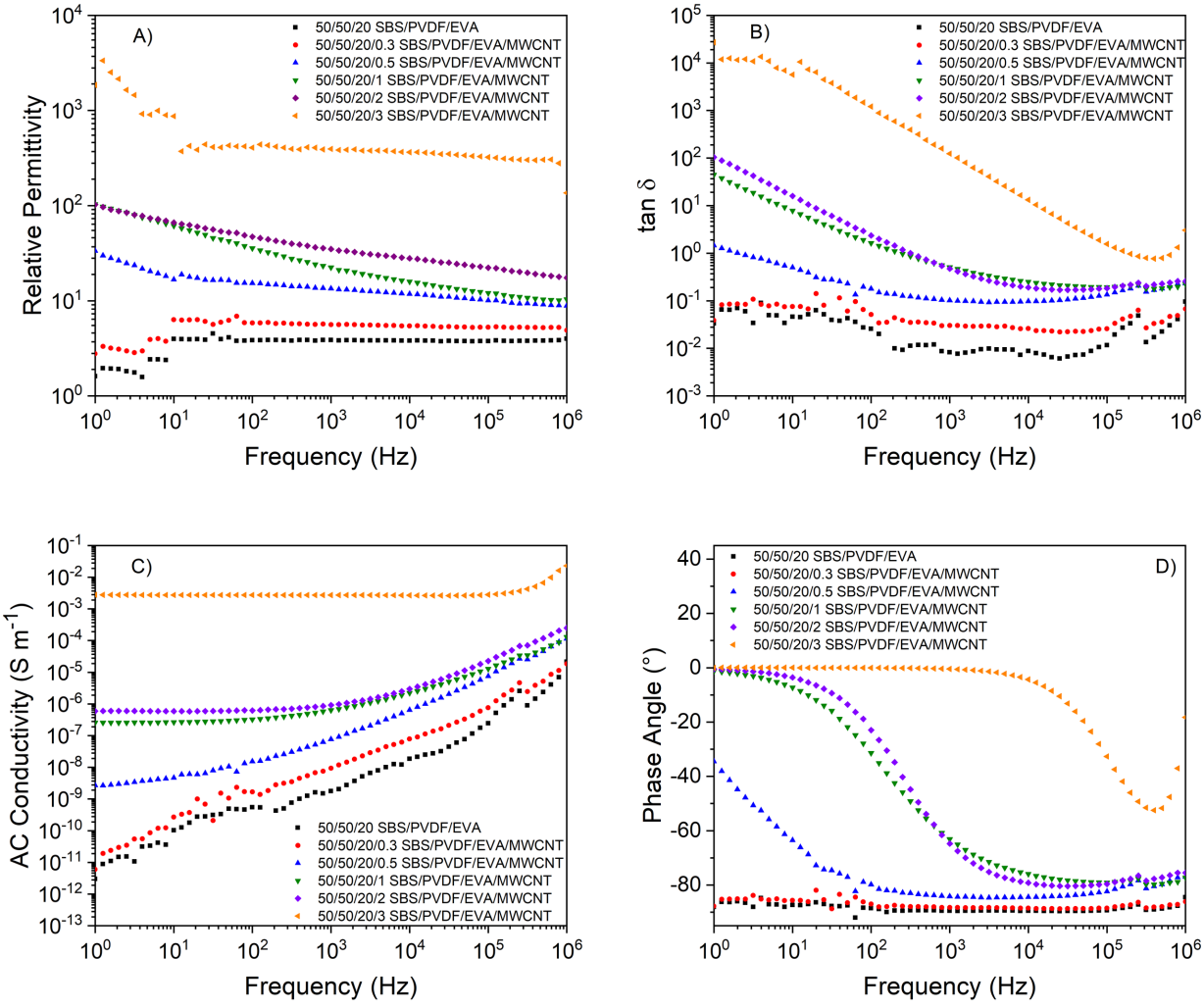

Figure 7: A) relative permittivity, B) *tan δ*, C) AC conductivity and D) phase angle of SBS/PVDF/EVA (50/50/20) and MWCNT containing composites.

Figure 8 shows the polarisation-field (P-E) loops of all the samples tested. As shown in Figure 8A, the SBS/PVDF/EVA sample with no MWCNT filler exhibited straight and linear polarisation-field loops, which indicates the material acting as a simple dielectric capacitor (*C*) since *Q*=*CV* and the charge, *Q*, is related to the y-axis (polarisation) and the voltage, *V*, is related to the x-axis

(electric field). This is in agreement with the low loss and phase angle of 90° in Figure 7B and D respectively; however these measurements are at much higher electric fields. Figure 8B shows that the sample containing 0.3 wt% MWCNT exhibits a less linear and more open polarisation-field loop. Such a response is typical of a 'lossy dielectric' due to the presence of some electrical conductivity in the sample and is not due ferroelectric properties.[38] Figure 8C both show that samples with higher MWCNT content (0.5 wt%) exhibit a more circular polarisation-field loop; and this indicates that the material is moving from the lossy dielectric response in Figure 8B to a conductor, and indicates the percolation of MWCNT in the material, as indicated by the rise in AC conductivity in Figure 7B. Finally Figure 8D shows the sample containing 1 wt% MWCNT. This shows that the sample is conducting even at low fields and has moved completely away from a lossy dielectric response to a circular polarisation-field loop.

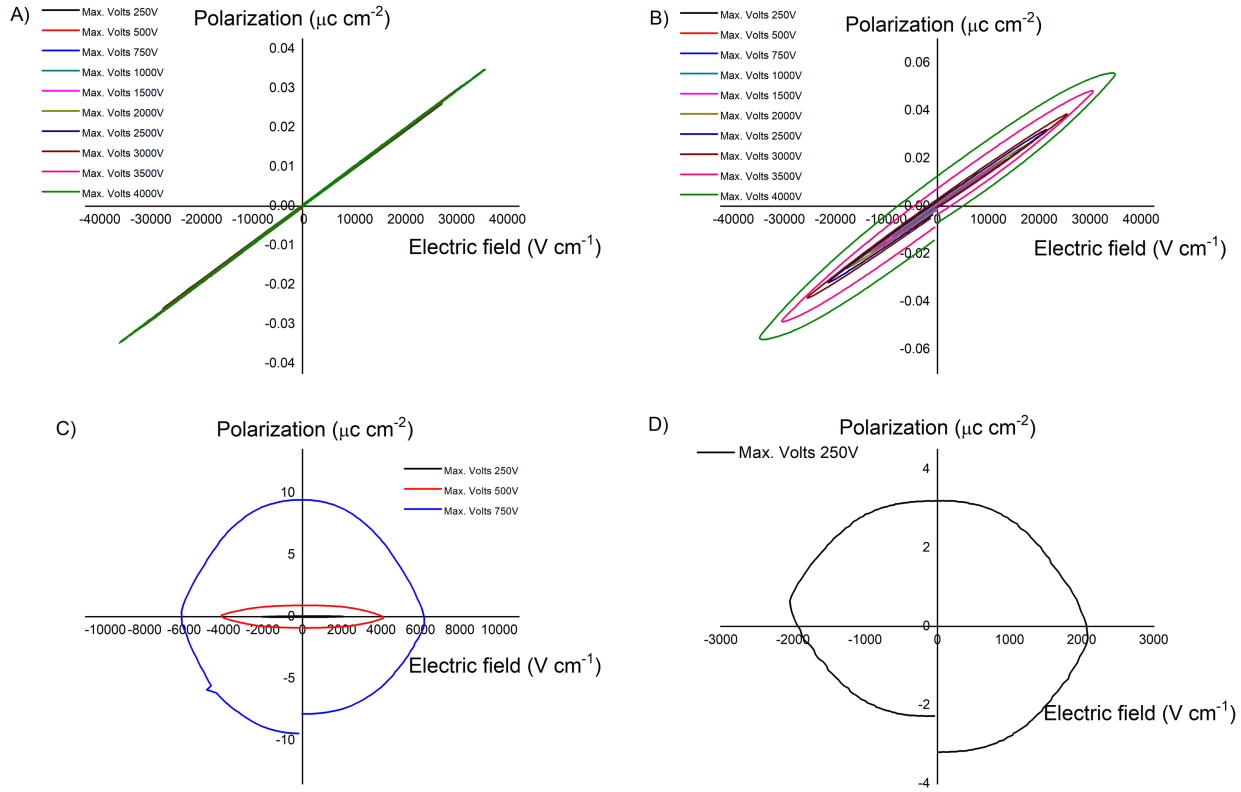

Figure 8: Polarisation- electric field (P-E) loop data of SBS/PVDF/EVA containing MWCNT of (A) 0 wt%, (B) 0.3 wt%, (C) 0.5 wt% and (D) 1 wt% MWCNT.

Electrical dual percolation under mechanical stretching

To understand to change in microstructure and electrical properties during deformation the capacitance (C) and phase angle (θ) was measured as a function of frequency as the material was strained, as shown Figure 9. During deformation there is likely to be changes in both sample geometry and microstructure; therefore C and θ were monitored since capacitance is dependent on sample geometry and microstructure (since $C = \frac{(A\varepsilon_r\varepsilon_0)}{t}$), while phase angle is only dependent on microstructure and insensitive to changes in geometry (since $\theta = tan^{-1}\left(\frac{Z''}{Z'}\right)$; where Z' is the real impedance and Z'' is the imaginary impedance).

For the SBS/PVDF/EVA blend, Figure 9A, the capacitance is relatively frequency independent at low frequencies and this is due to the material simply acting as a dielectric; a small relaxation at higher frequencies is observed. This also can be seen in Figure 9B, with a phase angle of ~90° at low frequency. The capacitance increases with strain in Figure 9A, and this is primarily due to material thickness decreasing with increasing tensile strain; this is also reflected in the limited change in phase angle in Figure 9B.

The SBS/PVDF/EVA composite with 1 wt% MWCNT is above the first percolation threshold with MWCNTs only in the continuous SBS phase. The capacitance is highly frequency dependent at low frequencies, Figure 9C, and this is due to the presence of electrical conductivity[39] due to percolation of MWCNTs in the SBS phase. This can also be observed in the phase angle which moves towards 0° at low frequency, see Figure 9D. The low frequency region does not change significantly with strain and this may indicate that the percolated network of MWCNTs has not changed to any significant extent during deformation. The intermediate frequency region behaves similarly to the response seen for SBS/PVDF/EVA, Figure 9A, with a frequency plateau in capacitance and a small relaxation at higher frequencies. Interestingly, the capacitance is most dependent on strain in this intermediate frequency region (10^2-10^3 Hz) where the phase angle approaches ~90°. For this material, the change in phase angle with strain in Figure 9D indicates a change in the microstructure during deformation.

The SBS/PVDF/EVA with 3 wt% of MWCNT is above the second percolation threshold for both the SBS and PVDF phase, and the capacitance does not vary significantly with deformation up to its elongation at break. This is likely to be due to the percolation network of MWCNTs throughout the composite being unaffected by strain, Figure 9E. The high degree of percolation in this composite is indicated by the phase angle approaching 0° at low frequencies, Figure 9F.

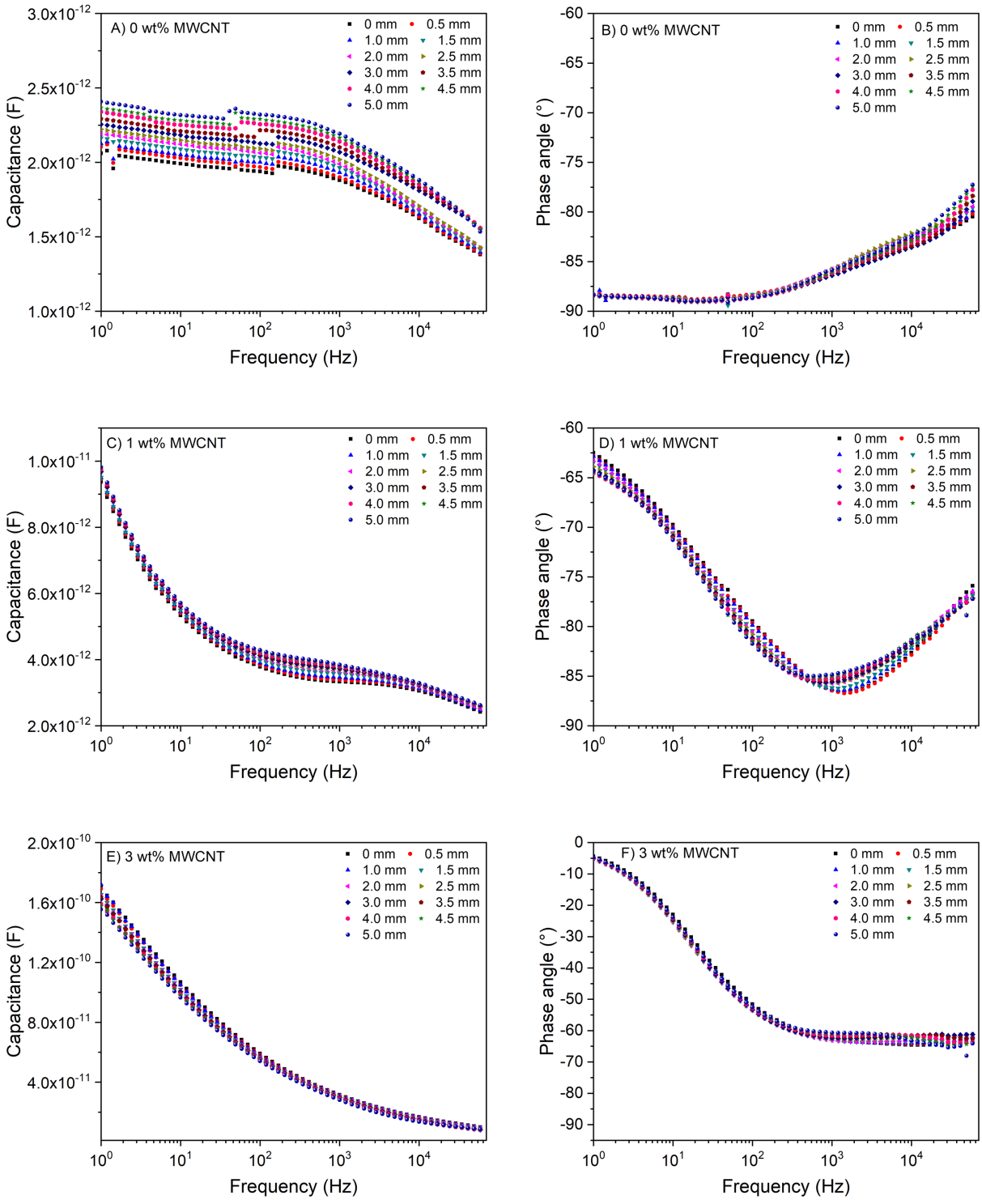

Figure 9: Variation in capacitance with extension for SBS/PVDF/EVA TPEs containing MWCNTs of (A) 0 wt%, (C) 1 wt% and (E) 3 wt%. Variation in phase angle with extension for the TPEs containing MWCNTs of (B) 0 wt%, (D) 1 wt% and (F) 3 wt%.

We can now put forward a mechanism to understand these responses considering the material as a dual percolated composite and as a resistor-capacitor network,[40] where the resistor (*R*) represents the conductive phase and the capacitor (*C*) represents the capacitive phase. As shown in Figure 10A, in the SBS/PVDF/EVA composite with 1 wt% MWCNT above the first percolation threshold, the composite can be considered as a conductive SBS containing percolated MCNWTs (which acts as the resistor, *R*) along with discrete islands of insulating PVDF with no percolated MWCNT (which acts as the capacitor, *C*). At low frequencies (*f*) the AC currents will flow thorough the conductive SBS matrix, since $R^{-1} >> 2\pi fC$, and the phase angle approaches 0° (see Figure 9C and E). At higher frequencies the AC conductivity of the capacitive regions increases and when $R^{-1} \sim 2\pi fC$, the capacitive PVDF regions contribute to the AC currents so that the phase angle approaches 90° as the frequency increases. If the 1 wt% composite material is initially unstrained the PVDF layers can be considered to be relatively low capacitance (since they have a relatively high thickness). As the material is deformed and aligned in the direction of strain, the thickness of the PVDF islands will decrease and their capacitance is increased; as a result the condition $R^{-1} \sim 2\pi fC$ is observed at lower frequencies for the strained material. This can be seen in Figure 9D where the frequency of minimum phase angle (~ 90°) is achieved at increasingly lower frequencies as the material is deformed. For the SBS/PVDF/EVA composite with 3 wt%, the material is above the second percolation threshold and both the SBS and PVDF phases are conductive and therefore the structure consists of a purely resistive network, as shown in Figure 10B. In this case, no significant changes in capacitance and phase angle are observed with strain, and the limited change in electrical properties of this fully percolated 3 wt% MWCNT material during deformation indicates that the MWCNT network is relatively unaffected for the strain levels up to its elongation at break (~30%).

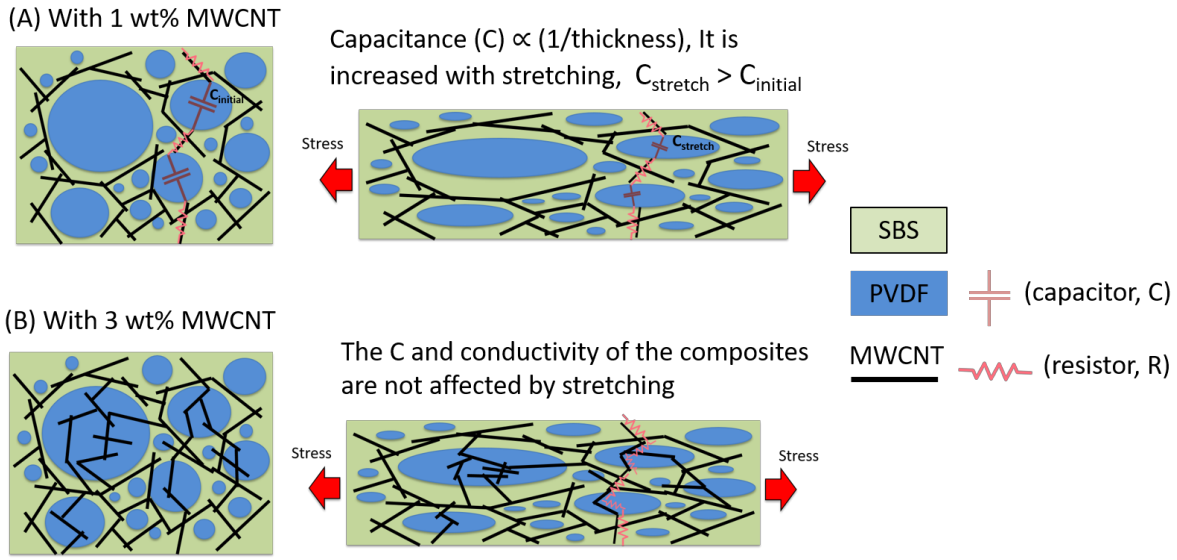

Figure 10 Schematic of dual the percolated composite working as a resistor-capacitor network under mechanical stretching

Conclusions

This work reports the formation and structure-property characterisation of stretchable thermoplastic elastomer (TPE) composites of EVA-compatibilised SBS/PVDF blends and MWCNTs. The addition of 20 wt% of EVA significantly altered the phase morphology, and resulted smaller PVDF phases dispersed in the SBS matrix.

The EVA compatibilisation of SBS/PVDF system also helped to achieve good stretchability of the blend, but also led to changes in the α- to β-phase ratio of crystallinity. In neat PVDF, the β-phase has a greater intensity than α-phase crystallinity. However, by blending with SBS and EVA, the α-phase increased to become more dominant, while the β-phase decreased - some of the β-phase was converted to α-phase crystallinity whilst some regions became amorphous as observed by the decrease in degree of crystallinity, as shown by DSC. An initial rheological percolation threshold for the MWCNTs was achieved between 0.5 and 1 wt%, with a second percolation event between 2 and 3 wt%.

A dual-percolation in electrical and rheological behaviour was found for the composite systems, and was driven by the content and localisation of MWCNTs within respective blend phases. Particularly, the first percolation threshold was reached within the SBS phase at lower loadings of

MWCNT (1-2 wt %), and led to relatively modest increases in the dielectric permittivity (ε_r ~ 23-35 at 10^3 Hz). The inclusion of 3 wt% of MWCNT led to the second percolation event (localisation of a MWCNT network in the PVDF/EVA phase), and caused a significant increase in relative permittivity of around ε_r ~ 395.0 (at 10^3 Hz), and recording a large *tan* δ of 123.8. The existence of a double electrical percolation threshold in the composites was further supported by the changes in the AC conductivity and phase angle between all of the samples. Changes in the dielectric properties of materials above the first percolation threshold are due to the non-percolated PVDF islands acting as variable capacitors, whose capacitance increases with degree of stretching as the phase dimension becomes thinner.

In general, the composite system reported in this work results in a good combination of mechanical properties, and high relative permittivity, whilst maintaining a low dielectric loss. The combination of high permittivity, low dielectric loss and appropriate mechanical properties means that the EVA-compatibilised SBS/PVDF TPE composite systems can be considered as a suitable material system for vibration control sensors, variable impedance devices, energy harvesters and artificial muscles and actuators.

ACKNOWLEDGMENT

First author (CE) thanks EPSRC and Jaguar Land Rover (UK) for funding this PhD studentship through the iCASE award. Third author (XY) thanks China Scholarship Council for funding.

References

[1] C. Ellingford, C. Bowen, T. McNally, C. Wan, Intrinsically Tuning the Electromechanical Properties of Elastomeric Dielectrics: A Chemistry Perspective, Macromol. Rapid Commun. 39(18) (2018) 1800340.

[2] R.D. Kornbluh, R. Pelrine, Q. Pei, R. Heydt, S. Stanford, S. Oh, J. Eckerle, Electroelastomers: applications of dielectric elastomer transducers for actuation, generation, and smart structures, SPIE's 9th Annual International Symposium on Smart Structures and Materials, SPIE, 2002, p. 17.

[3] D.M. Opris, Polar Elastomers as Novel Materials for Electromechanical Actuator Applications, Adv. Mater. 30(5) (2018) 1703678.

[4] F.B. Madsen, A.E. Daugaard, S. Hvilsted, A.L. Skov, The Current State of Silicone-Based Dielectric Elastomer Transducers, Macromol. Rapid Commun. 37(5) (2016) 378-413.

[5] R. Pelrine, R. Kornbluh, Q. Pei, J. Joseph, High-Speed Electrically Actuated Elastomers with Strain Greater Than 100%, Science 287(5454) (2000) 836-839.
[6] M. Rabuffi, G. Picci, Status quo and future prospects for metallized polypropylene energy storage capacitors, IEEE Trans. Plasma Sci. 30(5) (2002) 1939-1942.
[7] J. Song, G. Zhao, B. Li, J. Wang, Design optimization of PVDF-based piezoelectric energy harvesters, Heliyon 3(9) (2017) e00377.
[8] L.F. Malmonge, S.d.C. Langiano, J.M.M. Cordeiro, L.H.C. Mattoso, J.A. Malmonge, Thermal and mechanical properties of PVDF/PANI blends, Materials Research 13 (2010) 465-470.
[9] C. Ellingford, C. Wan, Ł. Figiel, T. McNally, Mechanical and dielectric properties of MWCNT filled chemically modified SBS/PVDF blends, Composites Communications 8 (2018) 58-64.
[10] X. Jiang, C. Xu, Y. Wang, Y. Chen, Polyvinylidene Fluoride/Acrylonitrile Butadiene Rubber Blends Prepared Via Dynamic Vulcanization, Journal of Macromolecular Science, Part B 54(1) (2015) 58-70.
[11] Y. Li, Y. Oono, Y. Kadowaki, T. Inoue, K. Nakayama, H. Shimizu, A Novel Thermoplastic Elastomer by Reaction-Induced Phase Decomposition from a Miscible Polymer Blend, Macromolecules 39(12) (2006) 4195-4201.
[12] N. Moussaif, R. Jérôme, Compatibilization of immiscible polymer blends (PC/PVDF) by the addition of a third polymer (PMMA): analysis of phase morphology and mechanical properties, Polymer 40(14) (1999) 3919-3932.
[13] D. Li, S. Song, C. Li, C. Cao, S. Sun, H. Zhang, Compatibilization effect of MMA-co-GMA copolymers on the properties of polyamide 6/Poly(vinylidene fluoride) blends, J. Polym. Res 22(6) (2015) 102.
[14] D. Kuang, R. Li, J. Pei, Polyamide 11/poly (vinylidene fluoride)/vinyl acetate-maleic anhydride copolymer as novel blends flexible materials for capacitors, Polymers 6(8) (2014) 2146-2156.
[15] H. Ma, Y. Yang, Rheology, morphology and mechanical properties of compatibilized poly(vinylidene fluoride) (PVDF)/thermoplastic polyurethane (TPU) blends, Polym. Test. 27(4) (2008) 441-446.
[16] H. Mutsuda, J. Miyagi, Y. Doi, Y. Tanaka, H. Takao, Y. Sone, Flexible piezoelectric sheet for wind energy harvesting, Int. J, Energy Eng. 4(2) (2014) 67.

[17] X.-l. Xu, C.-j. Yang, J.-h. Yang, T. Huang, N. Zhang, Y. Wang, Z.-w. Zhou, Excellent dielectric properties of poly(vinylidene fluoride) composites based on partially reduced graphene oxide, Composites, Part B 109 (2017) 91-100.
[18] M. Li, Y. Deng, Y. Wang, Y. Zhang, J. Bai, High dielectric properties in a three-phase polymer composite induced by a parallel structure, Mater. Chem. Phys. 139(2) (2013) 865-870.
[19] J.I. Roscow, C.R. Bowen, D.P. Almond, Breakdown in the Case for Materials with Giant Permittivity?, ACS Energy Lett. 2(10) (2017) 2264-2269.
[20] I. Otero-Navas, M. Arjmand, U. Sundararaj, Carbon nanotube induced double percolation in polymer blends: Morphology, rheology and broadband dielectric properties, Polymer 114 (2017) 122-134.
[21] Z. Cheng, H.-F. Han, X.-S. Yi, S. Asai, M. Sumita, Selective location of the filler and double percolation of Ketjenblack filled High Density Polyethylene/Isotactic Polypropylene blends, Compos. Interfaces 6(3) (1998) 227-236.
[22] S.J. Chin, S. Vempati, P. Dawson, M. Knite, A. Linarts, K. Ozols, T. McNally, Electrical conduction and rheological behaviour of composites of poly(ε-caprolactone) and MWCNTs, Polymer 58 (2015) 209-221.
[23] L. Keun Yoon, B. Kyu Kim, Compatibility of poly(vinylidene fluoride) (PVDF)/polyamide 12 (PA12) blends, J. Appl. Polym. Sci. 78(7) (2000) 1374-1380.
[24] M.H. Lang, J. Zhang, Morphology and properties of poly(vinylidene fluoride) (PVDF)/ethylene–vinyl acetate copolymer (EVA) blends, Plastics, Rubber and Composites 43(1) (2014) 8-14.
[25] R.-C. Zhang, Y. Xu, Z. Lu, M. Min, Y. Gao, Y. Huang, A. Lu, Investigation on the crystallization behavior of poly(ether ether ketone)/poly(phenylene sulfide) blends, J. Appl. Polym. Sci. 108(3) (2008) 1829-1836.
[26] J. Chen, Y.-y. Shi, J.-h. Yang, N. Zhang, T. Huang, C. Chen, Y. Wang, Z.-w. Zhou, A simple strategy to achieve very low percolation threshold via the selective distribution of carbon nanotubes at the interface of polymer blends, J. Mater. Chem. 22(42) (2012) 22398-22404.
[27] D.K. Owens, R.C. Wendt, Estimation of the surface free energy of polymers, J. Appl. Polym. Sci. 13(8) (1969) 1741-1747.
[28] L. Cao, S. Deng, Z. Lin, Enhancement of Carbon Nanotube Particle Distribution in PPS/PEEK/Carbon Nanotube Ternary Composites with Sausage-Like Structure, Polymers 8(2) (2016) 50.

[29] L. Zonder, S. McCarthy, F. Rios, A. Ophir, S. Kenig, Viscosity Ratio and Interfacial Tension as Carbon Nanotubes Distributing Factors in Melt-Mixed Blends of Polyamide 12 and High-Density Polyethylene, Adv. Polym. Tech. 33(4) (2014).
[30] L. Lu, Z. Zhou, Y. Zhang, S. Wang, Y. Zhang, Reinforcement of styrene–butadiene–styrene tri-block copolymer by multi-walled carbon nanotubes via melt mixing, Carbon 45(13) (2007) 2621-2627.
[31] S. Inukai, K.-i. Niihara, T. Noguchi, H. Ueki, A. Magario, E. Yamada, S. Inagaki, M. Endo, Preparation and Properties of Multiwall Carbon Nanotubes/Polystyrene-Block-Polybutadiene-Block-Polystyrene Composites, Ind. Eng. Chem. Res. 50(13) (2011) 8016-8022.
[32] S. Yu, X. Wang, H. Xiang, L. Zhu, M. Tebyetekerwa, M. Zhu, Superior piezoresistive strain sensing behaviors of carbon nanotubes in one-dimensional polymer fiber structure, Carbon 140 (2018) 1-9.
[33] X. Wang, S. Meng, M. Tebyetekerwa, Y. Li, J. Pionteck, B. Sun, Z. Qin, M. Zhu, Highly sensitive and stretchable piezoresistive strain sensor based on conductive poly(styrene-butadiene-styrene)/few layer graphene composite fiber, Composites Part A: Applied Science and Manufacturing 105 (2018) 291-299.
[34] V. Kochervinskii, I. Malyshkina, N. Gavrilova, S. Sulyanov, N. Bessonova, Peculiarities of dielectric relaxation in poly(vinylidene fluoride) with different thermal history, J. Non-Cryst. Solids 353(47) (2007) 4443-4447.
[35] X.M. Shi, J. Zhang, J. Jin, S.J. Chen, Non-isothermal crystallization and melting of ethylene-vinyl acetate copolymers with different vinyl acetate contents, Express Polymer Letters 2 (2008) 623-629.
[36] K. Ke, Y. Wang, K. Zhang, Y. Luo, W. Yang, B.-H. Xie, M.-B. Yang, Melt viscoelasticity, electrical conductivity, and crystallization of PVDF/MWCNT composites: Effect of the dispersion of MWCNTs, J. Appl. Polym. Sci. 125(S1) (2012) E49-E57.
[37] Z. Chen, L. Xie, X. Huang, S. Li, P. Jiang, Achieving large dielectric property improvement in polymer/carbon nanotube composites by engineering the nanotube surface via atom transfer radical polymerization, Carbon 95 (2015) 895-903.
[38] J.F. Scott, Ferroelectrics go bananas, J. Phys.: Condens. Matter 20(2) (2008) 021001.
[39] D.P. Almond, C.R. Bowen, An Explanation of the Photoinduced Giant Dielectric Constant of Lead Halide Perovskite Solar Cells, The Journal of Physical Chemistry Letters 6(9) (2015) 1736-1740.

[40] D.P. Almond, C.R. Bowen, Anomalous Power Law Dispersions in ac Conductivity and Permittivity Shown to be Characteristics of Microstructural Electrical Networks, Phys. Rev. Lett. 92(15) (2004) 157601.